Ann. Phys. (Berlin) 527, No. 11–12, 806–813 (2015) / DOI 10.1002/andp.201500229

annalen der physik

Original Paper

Electrochemical structure-switching sensing using nanoplasmonic devices

Sergiy Patskovsky[1,*], *Anne-Marie Dallaire*[1], *Andre-Pierre Blanchard-Dionne*[1], *Alexis Vallée-Bélisle*[2], *and Michel Meunier*[1]

Received 1 July 2015, revised 28 September 2015, accepted 13 October 2015
Published online 3 November 2015

In this article, the implementation of electrochemical plasmonic nanostructures functionalized with DNA-based structure-switching sensors is presented. eNanoSPR devices with open and microfluidic measurement cells are developed on the base of nanohole arrays in 100 nm gold film and applied for combined microscopic and electrochemical surface plasmon (eSPR) visualization. eSPR voltammograms and spectroscopy are performed using planar three electrode schematic with plasmonic nanostructure operated as working electrode. Limit of detection of eNanoSPR devices for oligonucleotide hybridization is estimated in the low nanomolar and applications for structure-switching electro-plasmonic sensing in complex liquids are discussed.

1 Introduction

Continuous, real-time monitoring of specific small molecules in complex, unprocessed aqueous samples is very important for a broad spectrum of demanding applications ranging from medical diagnostics to environmental monitoring. Ideal sensor needs to be label-free, sensitive, stable, and selective enough to deploy directly in complex sample matrices. Surface plasmon resonance (SPR) is one of the most sensitive label-free detection techniques for real-time study of molecular interactions. However, wide spreading of this technology is impeded by a high level of nonspecific responses in crude samples due to the confounding effects of nonspecific adsorption to sensor surface [1]. In contrast, structure-switching sensors based on binding-induced conformational changes in a biomolecule have proven selective enough to work directly in many unprocessed aqueous samples [2, 3]. In such case, the nonspecific binding of contaminants does not trigger the specific conformational change in the biomolecule due to lack of precise molecular recognition. Another advantage of structure-switching sensors is that their binding induced conformational change can be readily adapted to generate an electrochemical signal using electroactive redox tags with a potential range which a rarely found in contaminants. Here we proposed to combine the performance of structure-switching sensors with the high sensitivity of SPR sensing in plasmonic-based electrochemical biosensing (eSPR). SPR is an optical method that detects changes in refractive index near a plasmon supporting metal surface. Such changes can be generated by fluctuation of surface charge density due to the local electrochemical reaction and detected [4] or even imaged [5] by eSPR. Thus, the eSPR method allows for simultaneous SPR and electrochemical analysis of molecular binding processes and is less sensitive to bulk refractive index changes or nonspecific binding than conventional SPR [6]. Electrochemical plasmonic sensing can be realized on nanoplasmonic structures [7–10] that offer multiplexing capability with high sensitivity and low detection limit [11], micro and flow-throw fluidic [12] approaches. Key advantages of the nanoplasmonic sensors are their potential to simplify optical systems design, to achieve multiplexed detection by spatial translation or by spectral separation and their ease of integration with portable and disposable sensing chips. In the article we evaluate the feasibility of combined electrochemical structure-switching and nanoplasmonic sensing based on nanohole arrays. We propose a design of eNanoSPR chips for analytical applications where main advantages of nanoplasmonic sensing – namely

* Corresponding author E-mail: sergiy.patskovsky@polymtl.ca
[1] Department of Engineering Physics, Laser Processing and Plasmonics Laboratory, Polytechnique, Montréal, P.O. 6079, Station Centre-ville, QC, H3C 3A7, Canada
[2] Laboratory of Biosensors and Nanomachines, Département de Chimie, Université de Montréal, Montréal (Québec), Canada

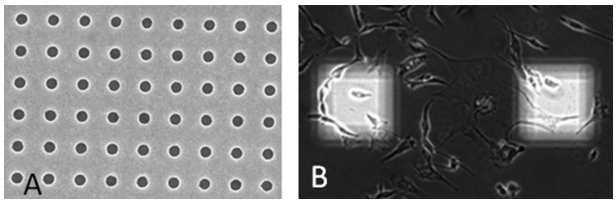

Figure 1 (A) SEM of the nanohole array with a hole diameter of 150 nm and periodicity of 450 nm. (B) Microscopy image of the gold nanohole arrays (100 μm $\times$ 100 μm) with fixed MDA-MB-231 cells.

wide-field microscopy and microfluidic biosensing – can be fully realized.

2 Experimental section

2.1 Chemicals and materials

Oligonucleotides were purchased from Biosearch Technologies (Petaluma, CA). Oligonucleotide probe P2 (5′ HS-MC6 – act ctc caa gcg ccg act gtt gag agg -MB 3′) contains a sequence complementary to the rpoB gene of *Mycobacterium Tuberculosis* associated with drug resistant tuberculosis. It was modified at its 5′ end with a thiol group to promote immobilization to the gold surface and at its 3′ end with a methylene blue (MB) reporter. This structure-switching oligonucleotide was designed to adopt a stem-loop conformation with a 5 base pair stem. The target T2 (5′ tc aa cag tcg gcg ctt gg 3′) is complementary to the loop sequence in P2. Tris(carboxyethyl)phosphine (TCEP), saline-sodium citrate (SSC) buffer and all other reagents were obtained from Sigma Aldrich.

2.2 Fabrication of nanohole array structure

150 nm diameter nanohole array with periodicities 375, 400, 425, 450, 475 nm and size 100 μm $\times$100 μm, were fabricated using electron-beam lithography in a lift-off process, using a cross-linked PMMA resist bilayer (negative tone) as a deposition mask (Figure 1A). A first layer of 170 nm 950k PMMA 2% in anisole (MicroChem) was spun onto a glass substrate covered with a 100 nm Indium Tin Oxide (ITO) layer (Sigma Aldrich) using a Brewer Science 200cbx spin coater. A second layer of 400 nm 450k PMMA 4% in anisole (MicroChem) is spun on top of the first layer. Having a higher molecular weight, the dose required to crosslink the bottom layer is higher, resulting in a slightly underexpose layer, which creates an undercut for the lift-off process. The bilayer was then patterned using electron beam lithography at a dose of 10 mC/cm^2 using a Raith eLine Plus system at an acceleration voltage of 20 kV. Development of the resist is achieved by gently agitating the sample manually in acetone for about 180 seconds. The sample is then placed in a high vacuum chamber inside an Edwards electron beam evaporator where a 100 nm gold layer is deposited on top of the pattern. Dry etching of the underlying resist is achieved by an O2 plasma at 500 W at a pressure of 200 mTorr for 15 minutes using a PVA Tepla GIGAbatch 310 plasma asher. The sample is then rinsed in acetone in an ultrasonic bath for about 5 minutes to remove any undesirable etching residues.

2.3 Structure-switching sensor preparation

Prior to functionalization, slides with nanohole arrays were cleaned by the oxygen plasma cleaner, rinsed in MilliQ water and dried under a N_2 flow. Probe oligonucleotides were immobilized on the sensor surface using thiol-gold chemistry following a protocol previously described [13]. To reduce disulfide bonds between the thiol-modified probes, 2 μL of 100 μM probe were incubated with 4 μL of 10 mM TCEP for an hour at 4°C then diluted in PBS to obtain a probe concentration of 650 nM. A 200 μL drop of this solution was then placed on the gold chip and left to incubate for an hour in a humid chamber. The chip was then rinsed with water then incubated in a solution of 2 mM 6-mercapto-1-hexanol (MCH) in PBS at 4°C overnight. MCH is used to fill the free sites on the gold and has three main functions: block the surface from non-specific adsorption, prevent the oligonucleotide probes from lying on the surface and passivate the electrode. Before testing, the chip was rinsed with water and let to equilibrate in 2xSSC for 10 minutes.

2.4 Apparatus and measurement

Our experimental set-up is shown in Figure 2. The optical system was built on the base of Nikon Ti inverted microscope equipped with a 50W halogen light source and an imaging spectrophotometer (Andor). A supercontinuum laser (Fianium) coupled to an optical filter (Photon Etc) served as a tunable narrow (4 nm) band light source. Electrochemical measurements were performed by a potentiostat (Solartron Analytical) wired to the sample by a three electrodes schematic. A platinum disk (1 cm diameter) and an Ag/AgCl electrode filled with 3 M KCl electrolyte were used respectively as a counter-electrode and as a reference electrode. Electro-optical responses

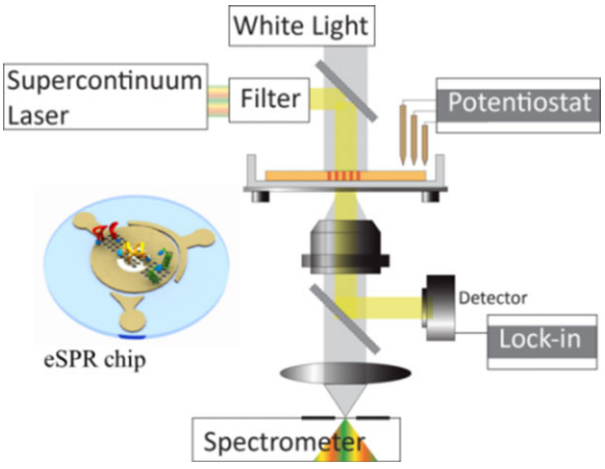

Figure 2 Schematic of the experimental set-up and eSPR biosensing chip.

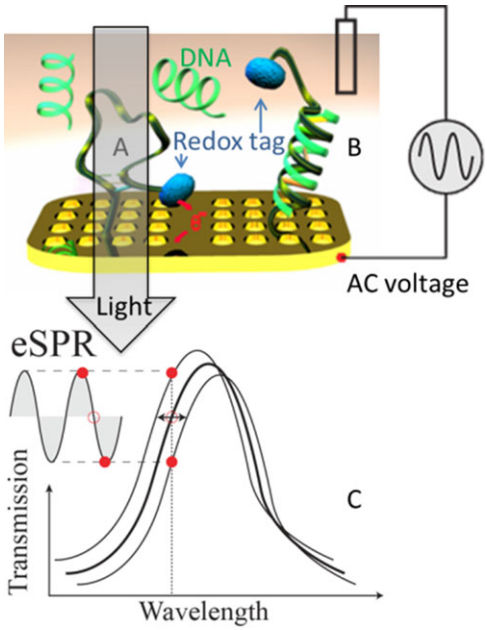

Figure 3 eSPR principle of structure-switching sensing using nanoplasmonic devices. Structure-switching sensor with redox tag close to the surface (A) and far from the surface (B) after DNA hybridization. (C) Modulated by AC voltage nanoholes resonance transmission spectrum.

of nanoplasmonic structures to the voltage modulations were measured by an amplified detector (Thorlabs) connected to a lock-in amplifier (SR830, Stanford Research Systems).

Real time monitoring of the light spectrum transmitted through the nanohole array was used for the nanostructure plasmonic characterization and evaluation of its sensitivity to the bulk refractive index (RI) changes. Homemade software based on *LabView* calculated spectral position of the resonance peak, its maximum intensity and displayed dynamic of the biosensing response.

The eSPR method used in this work is similar to the electrochemical plasmonic sensing technique [6]. In the case where the surface of the sensor chip is functionalized with electroactive redox tags, the applied potential will generate a variation of concentration for the oxidized and reduced species. As both species have different refractive indices, the monitored SPR response will also contain component associated with local RI fluctuation [14]. Spectro-electrochemical analysis of this phenomenon was experimentally realized with a conventional SPR system [15] and an optical waveguide platform [16, 17]. In this article, we investigate a structure-switching sensor that contains an electroactive redox tag – namely methylene blue – at one of its extremity. The sensors signalization is based on the selective binding to a complementary DNA target (Figure 3A) that induces conformational changes in structure-switching sensors and leads to increase of the distance between the redox tags (Figure 3B) and a conducting surface [18]. Redox electrochemical reaction becomes less probable, resulting in a decrease in the local RI modulation amplitude detectable by SPR that allows us to estimate target DNA concentration [6].

Experimentally, we apply on the nanoholes structure the constant potential and add an AC component at a 100 Hz frequency that is optimized for structure-switching sensors [13]. This perturbation generates a modulation of the transmitted resonance spectrum (Figure 3C). When we fix a wavelength of the transmitted light, the spectral modulation is transformed into an intensity modulation and its amplitude is measured by a lock-in amplifier. As a result, the eSPR response in our set-up is measured in volts and the phase information of the detected modulated signal is also available and can be used for evaluation of interfacial electrochemical parameters [19]. Several eSPR scanning modes can be realized by our set-up depending on the parameters of the experiments. First is eSPR AC Voltammetry, in which low-amplitude AC perturbations generate electro-optical plasmonic response detected at different DC potentials [20]. Second, a supercontinuum tunable light source available in our experimental set-up allows us to perform eSPR AC spectroscopy by scanning probing wavelength and fixing the applied DC voltage, usually at a potential that initiates a redox reaction (i.e. −0.275 mV for methylene blue). And third, dynamic eSPR measurements, where temporal dependences of eSPR responses at fixed wavelength and DC potential are obtained [6]. Due to the resonance nature of the

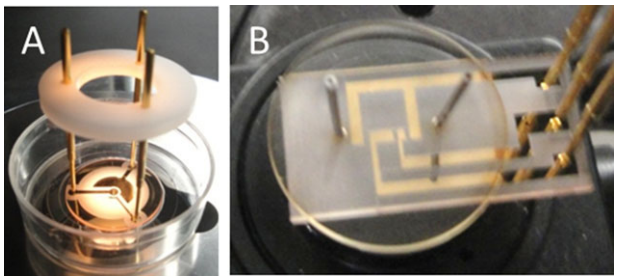

Figure 4 Photograph of eNanoSPR device with three planar electrodes for open (A) and microfluidic (B) measurement cell.

nanoplasmonic transmission spectra, the eSPR amplitude – and therefore the overall performance of eSPR devices – depends on the spectral position of the probing light. The information about optimal working wavelength and optimal redox DC potential for specific nanoholes structure with structure-switching sensor is obtained from corresponding eSPR AC Voltammetry and eSPR AC spectroscopy measurements.

2.5 Fabrication of microscopy eNanoSPR devices

Prototypes of eNanoSPR devices for microscopy applications with open and microfluidic measurement cell were fabricated using femtosecond laser micromachining system. A first eNanoSPR device was designed with a 1 mm^2 central working electrode with nine nanohole arrays, a closely separated reference electrode and a larger counter electrode (18 mm^2) shaped on a circular 18 mm BK7 glass substrate (Figure 4A). Such diameter allows a precise installation into petri dishes with glass bottom that are used for live cell microscopy. Spring loaded electrodes (Interconnect Devices) were wired to the potentiostat and provided contacts to the biosensing chip directly through liquid medium, greatly simplifying biosensing chip replacement. During measurements, the whole set-up is placed on a microscopy stage and the same light source is used for live cell imaging and nanohole array spectral and eSPR investigation.

A second eNanoSPR device for work with microfluidic was fabricated on a rectangular 12.5 mm × 25 mm glass substrate (Figure 4B). The three planar electrodes were long enough to accept contacting electrode from one side and to be embedded in a microfluidic channel with an area of 1 mm × 8 mm from another. The central working electrode patterned with nanoplasmonic structure has a size of 1 mm × 2 mm. The reference electrode is 1 mm × 0.5 mm and placed close to the working and both are enclosed by a larger counter electrode. The microfluidic chamber is formed by an O-ring cut from a 200 μm silicone sheet. An upper cover was made from circular 20 mm glass substrate 1 mm thick with two 1 mm drilled opening to allow liquid delivery to the sensing surface. Microfluidic eNanoSPR device can be installed on the same microscopy stage for visual and eSPR tests or used with independent simplified optical set-up comprising a LED light source and a silicon monodetector.

3 Results and discussion

A set of experimental transmission spectra in water medium for nanohole array samples with 150 nm diameter and 375, 400, 425, 450, 475 nm periodicities is presented on Figure 5A. We observed two distinctive resonance peaks related to the plasmonic enhancement of the electromagnetic wave at the gold-medium and the gold-substrate interface. Spectral peaks positions can be estimated by using an approximate equation for the free-space incident wavelength that excites a surface plasmon [21]:

$$\lambda_{SPR} = \frac{P}{\sqrt{s_1^2 + s_2^2}} \mathrm{Re}\sqrt{\frac{\varepsilon_{Au(\lambda_{SPR})}\varepsilon_m}{\varepsilon_{Au(\lambda_{SPR})} + \varepsilon_m}} \quad (1)$$

where (s_1, s_2) are integer pairs that correspond to the particular order of the SP mode, ε_m the relative dielectric constant of medium, and $\varepsilon_{Au(\lambda SPR)}$ is the complex wavelength-dependent dielectric constant of gold. Calculated λ_{SPR} dependences for metal interfaces with medium (water) and substrate (BK7 glass) on the nanohole array periodicities are presented on Figure 5B by dashed lines. For every resonance peak we found two characteristic parameters $\lambda(I_{min})$ and $\lambda(I_{max})$ corresponding to the spectral position at minimum and maximum intensity of the peak (Figure 5A). Results for all nanoplasmonic structures are shown on Figure 5B. We observed a rather good match between the $\lambda(I_{min})$ and the theoretical λ_{SPR} for Au-medium resonance mode. Spectral positions for $\lambda(I_{max})$ are red shifted for about 50 nm. This shift has to be considered to find the optimal combination of excitation light wavelength and nanohole array period applied for eSPR detection. $\lambda(I_{min})$ and $\lambda(I_{max})$ dependences for the peaks related to the Au-substrate interface demonstrated similar tendency but with larger red shifts. Such difference can be partially explained by approximation included in equation (1) that ignored coupling between top and bottom resonances of the metal film with limited thickness.

We have also verified the sensitivity of our nanoplasmonic structures in response to the bulk refractive

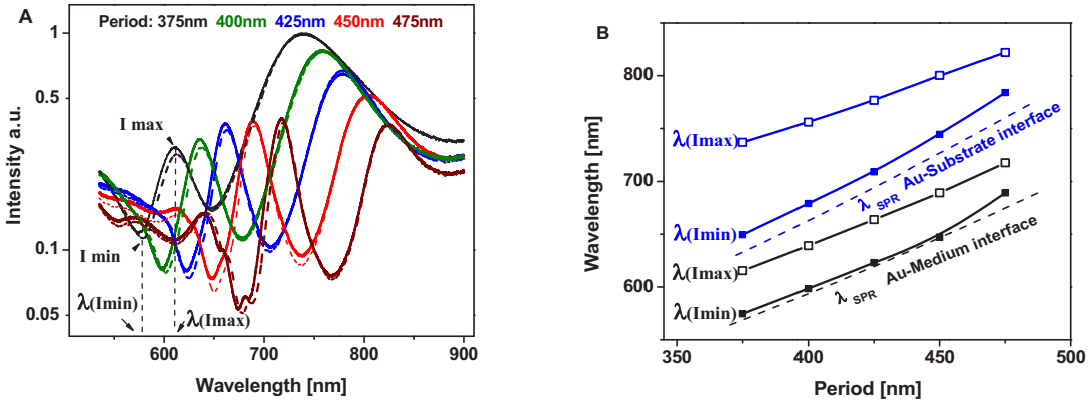

Figure 5 (A) Transmission spectra for gold nanohole arrays with diameter 150 nm and different periodicities from 375 nm to 475 nm. Dashed lines show spectra with 0.012RI bulk refractive index difference. I_{min} and I_{max} relate to the two extremities of the resonance peak. (B) Theoretical λ_{SPR} dependences on nanohole arrays periodicities for metal interfaces with medium (water) and glass substrate (dashed lines). Corresponding experimental spectral positions (full lines) for Imin and Imax.

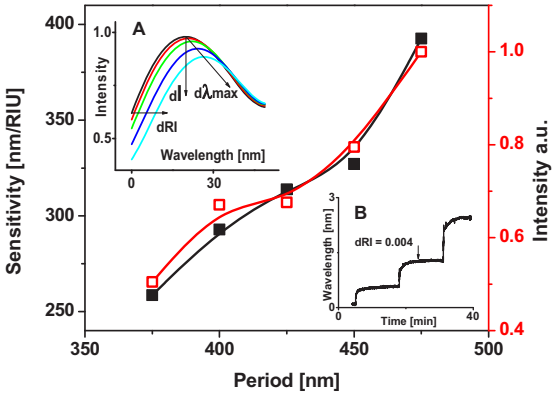

Figure 6 Spectral (black line) and intensity (red line) sensitivity to the bulk RI for different nanohole array periods. Inset (A) present direction of spectral and intensity shifts on RI increase. Inset (B) shows typical time dependence on the RI changes.

index changes. Ethanol-water solutions with different ratio and RI were delivered to the surface of the nanoplasmonic structure. Real-time transmission spectra were monitored and the dynamic of intensity and spectral position of the resonance peak were calculated. Examples of spectra shift upon increase on $1.2*10^{-2}$ RIU are shown as dashed lines on Figure 5A. As expected, larger shifts are observed for the first resonance peaks, whereas slight changes in the peak positions related to the Au-substrate interface can be explained by SPR coupling through 100 nm metal film and bulk RI changes inside nanoholes. On Figure 6 we present experimental spectral (black line) and intensity (red line) sensitivity to the bulk RI for different nanohole arrays. Inset (A) present typical behavior and direction of spectral and intensity shifts on bulk RI increase. Inset (B) shows example of typical time dependence on the RI changes.

As a model structure-switching electrochemical sensor, we used the well-characterized E-DNA sensor, which consists in a DNA stemloop [22] that contains an electroactive reporter methylene blue (MB) at one of its extremity and a thiol group at the other extremity to promote immobilization to the electrode surface. Upon binding to its complementary DNA sequence on its loop, this stemloop will undergo stem opening, which will separate the electroactive reporter from the electrode surface leading to a significant decrease in the electron transfer rate on thus measurable electrochemical signal. We can monitor the conformation of the stemloop, and thus the presence of the complementary target sequence, by using AC voltammetry [18]. Linear scanning of potential from 0 mV to −450 mV with added 50 mv 100 Hz AC signal results in a peak of current around −275 mV (*vs.* Ag/AgCl reference electrode filled with 3 M KCl electrolyte) associated with the redox activity of MB. The amplitude of this peak is correlated with the electron transfer efficiency between MB and the electrode and will vary according to the "on/off" state of the E-DNA switches.

In this article we are considering electro-plasmonic eSPR method for the redox reaction detection. The following experiments were performed on the nanoplasmonic structures functionalized with structure – switching sensor modified with methylene-blue redox reporter. eSPR spectroscopy measurements were executed for all nanostructures by scanning probing wavelength and fixing the applied DC voltage, and similar tendency was observed. Experimental results for gold nanohole array with periodicity 450 nm are presented on Figure 7. The

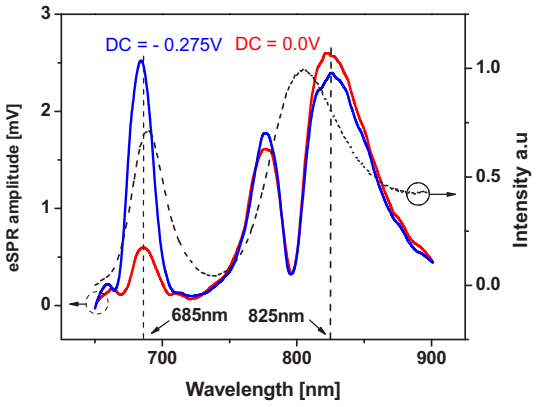

Figure 7 eSPR spectroscopy for gold nanohole array with periodicity 450 nm and functionalized with a model structure switching sensor (E-DNA). Red line corresponds to 0 V applied potential and blue line is obtained at redox potential −0.275 V. Black line shows transmission spectrum for comparison.

eSPR spectrum obtained with applied 0V potential is illustrated by a red line and obtained at MB reporter redox potential −0.275 V by a blue line. The black line shows conventional transmission spectra for comparison. As was explained above, eSPR method is based on the detection of electro-optical signal induced by small AC modulation and can be considered in our case as differentiation method of transmission spectra. It explains the fact that resonance peak related to the Au-substrate interface was transformed into double peak curve with maximums corresponding to the points of highest spectrum deviation. As shown in the literature [7], the optical spectrum of plasmon resonances in electrochemistry depends on multiple effects even in the absence of electron transfer reactions. However, in the case of Au-substrate interface we have no direct contact with solution. The existence and high intensity of detected eSPR response is attributed to modulation of electron density of the metal by an applied potential [23]. eSPR detection in this case could be used as an approach to investigate plasmonic coupling, and other parameters such as the Drude plasma frequency and other plasmonic phenomena localized at the Au-substrate interface. When applying a potential of −0.275 V (voltage for optimal electron transfer for MB), this causes a sharp increase in the eSPR intensity for the first resonance peak and, as expected, a much lower change for the second one (Figure 7, blue line). The eSPR spectral positions at peak maximum for all tested nanostructures typically deviated by 4–6 nm from corresponding values found for transmission spectra (Figure 5B). For example, for a nanohole array with 450 nm periodicity we observed resonance peak with maximum intensity positioned at 685 nm, and a narrow full width at half-maximum (FWHM) of about 20 nm. Corresponding data for transmission spectrum are 689 nm and 37 nm. Since transmission spectra shift due to the bulk RI changes usually is accompanied by amplitude change (Figure 6, inset (A)) eSPR spectrum at Au-medium interface shows only one strongly pronounced peak. For the following experiments we focused on this peak at 685 nm and for comparison we considered 825 nm corresponding to the resonance on Au-substrate interface.

Figure 8A shows the typical eSPR cyclic AC voltammograms obtained for gold nanohole array with a periodicity of 450 nm and functionalized with our model structure switching sensor (E-DNA). The potential was scanned from 0 to −0.45 V with 50 mV of AC amplitude at 100 Hz frequency. eSPR amplitude was monitored at 685 nm and 825 nm excitation wavelength. A very pronounced eSPR amplitude peak was obtained at −0.275 V confirming the presence of the MB reporter. Small peak was also observed for 825 nm excitation light and explained by the coupling resonances on metal surfaces and local RI fluctuations near nanoholes walls. For comparison, an electrochemical AC voltammogram is shown as a blue line. The observed results confirm the feasibility of eSPR method and allow us to consider nanohole array based structure – switching nanoplasmonic sensing for analytical applications.

Using our eNanoSPR devices we have performed experimental tests on hybridization between the E-DNA P2 and its complementary target T2. We used a 2×SSC running buffer concentration for the stage of hybridization. eSPR voltammograms for different concentrations of complementary oligonucleotide T2 and normalized to the peak value of the voltammograms in PBS are shown on Figure 8B. Real time results of P2-T2 hybridization at 300 nM T2 concentration is presented in the inset. The sensor surface can be used repeatedly by regeneration of bioselective element in 8 M urea solution [24]. The sensor demonstrated a reliable response to the P2-T2 hybridization with an estimated resolution of 10 nM T2 concentration. Final sensor sensitivity and resolution depend on the stability and noise of light source, total size of nanohole array, detector dynamic range and can be increased by recent technological solutions.

Scientists are always looking for new advanced methods or technologies relying on the combination of established approaches to improve the reliability and selectivity of label-free biosensing in complex aqueous samples. Examples include combination of quartz crystal microbalance and SPR method [25], SPR and impedance spectroscopy [26], dielectrophoresis and

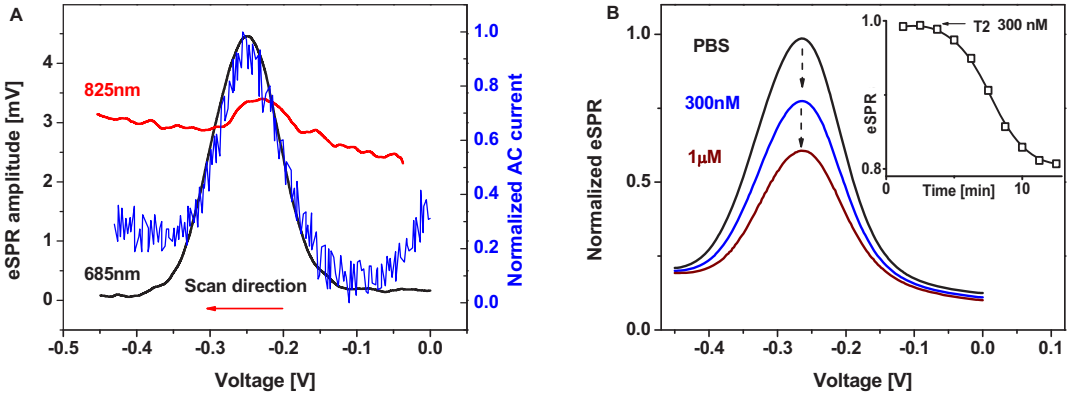

Figure 8 (A) eSPR cyclic AC voltammograms obtained for functionalized with structure switching sensor gold nanohole array with periodicity 450 nm. Scan was performed at 50 mv AC amplitude, frequency 100 Hz, 685 nm and 825 nm excitation wavelength. For comparison, an electrochemical AC voltammogram is shown (Blue line). (B) Normalized eSPR responses for hybridization tests between stemloop P2 and its complementary target T2. Inset: P2-T2 hybridization dynamic.

nanoplasmonic [27]. We believe that the combination of the sensitivity and multiplexing capability of nanoplasmonic structures together with the selectivity and robustness of structure-switching sensor to non-specific response represents an excellent avenue to develop reliable sensors for complex samples. We see several advantages of the proposed eSPR approach. It was already shown in literature [19] that electrochemical plasmonic sensing is less sensitive to bulk refractive index changes or nonspecific binding than conventional SPR. Also, eSPR approach activates and detects modulated response from reversible redox reactions whereas we expect no signal modulation from nonspecific biolayers or bulk RI variations. Influence of nonspecifics on the SPR resonance curve has to be rather big to influence eSPR modulation amplitude from redox reaction. And such influence can be recalibrated by measuring conventional SPR shift from DC level of eSPR response. The measurement protocol with differential channel for eSPR method will be more efficient that for conventional SPR as structure-switching sensing is immune to the nonspecific influences in complex media.

In this article, we present a prototype eNanoSPR device designed for sensing applications directly in complex media. Our eNanoSPR device for open measurement cell (Figure 4A) is compatible with a petri dish for live cell microscopy and allows cell growth on the nanostructure directly in the incubator. We expect that inverted microscopy set-up could be used to investigate metabolism of living cells by structure-switching eSPR sensors with direct visual monitoring. In Figure 1B, for example, we presented a microscopy image of the fixed MDA-MB-231 cells [28] attached to the surface of gold nanohole arrays (100 μm $\times$ 100 μm) fabricated in 100 nm thick gold film. Contrast of image is satisfactory for simultaneous cells and nanostructure visualization. Moreover, recent work on the nanohole arrays fabricated on the optically thin 50 nm metal film demonstrated satisfactory plasmonic properties with higher potential for imaging applications [29]. Electrochemical SPR detects RI changes that confined to the surface under illumination and thus less dependent on the total current passing through the system. We obtained very similar eSPR voltammograms for configuration with three planar electrodes fabricated on the same substrate and for the conventional configuration with Pt counter and Ag/AgCl reference electrodes. Planar electrodes are very suitable for microfluidic flow-injection eNanoSPR device configuration (Figure 4B). Such compact sensing system is compatible with microscopy but could be particularly advantageous for realizing a standalone portable device with multiplexed and disposable sensing chips for investigation of untreated blood samples.

4 Conclusions

In this paper, we described the development of eNanoSPR devices employing structure-switching sensor as a mediator to transduce an electrochemical reaction into measurable plasmonic response. Our eNanoSPR devices were based on a multiple gold nanohole arrays fabricated by e-beam and the vacuum deposition of a 100 nm gold film. We performed the synchronized measurement of optical spectral characteristics and cyclic eSPR voltammograms for the devices and estimated resolution using a model E-DNA sensor. Our eNanoSPR devices take advantages of nanoplasmonic

coupling at normal light incidence to realize combined nanoplasmonic multiplexing sensing with microscopic visualization. Proposed electrochemical structure-switching sensing using nanoplasmonic devices is promising for biosensing in the complex sample and shows a potential for the development of low-cost portable system with disposable sensing chips.

Acknowledgment. This work was supported by the Team research project program (Quebec, Canada).

Key words. Nanoplasmonics, structure-switching biosensors, optical sensors, microscopy.

References

[1] D. R. Walt, ACS Nano **3**, 2876 (2009).
[2] A. A. Lubin and K. W. Plaxco, Acc. Chem. Res. **43**, 496 (2010).
[3] A. Vallee-Belisle and K. W. Plaxco, Current opinion in structural biology **20**, 518 (2010).
[4] S. P. Wang, X. P. Huang, X. N. Shan, K. J. Foley, and N. J. Tao, Anal. Chem. **82**, 935 (2010).
[5] W. Wang, K. Foley, X. Shan, S. P. Wang, S. Eaton, V. J. Nagaraj, P. Wiktor, U. Patel, and N. J. Tao, Nat. Chem. **3**, 249 (2011).
[6] A.-M. Dallaire, S. Patskovsky, A. Vallée-Bélisle, and M. Meunier, Biosensors and Bioelectronics.
[7] A. B. Dahlin, B. Dielacher, P. Rajendran, K. Sugihara, T. Sannomiya, M. Zenobi-Wong, and J. Voros, Anal. Bioanal. Chem. **402**, 1773 (2012).
[8] K. Nakamoto, R. Kurita, and O. Niwa, Anal. Chem. **84**, 3187 (2012).
[9] A. P. Blanchard-Dionne, L. Guyot, S. Patskovsky, R. Gordon, and M. Meunier, Opt. Express **19**, 15041 (2011).
[10] S. P. Branagan and P. W. Bohn, Analyst **137**, 3932 (2012).
[11] A. E. Cetin, A. F. Coskun, B. C. Galarreta, M. Huang, D. Herman, A. Ozcan, and H. Altug, Light Sci. Appl. **3**, e122 (2014).
[12] F. Eftekhari, C. Escobedo, J. Ferreira, X. B. Duan, E. M. Girotto, A. G. Brolo, R. Gordon, and D. Sinton, Anal. Chem. **81**, 4308 (2009).
[13] A. A. Rowe, R. J. White, A. J. Bonham, and K. W. Plaxco, Journal of Visualized Experiments: JoVE, 2922 (2011).
[14] Y. Iwasaki, T. Horiuchi, M. Morita, and O. Niwa, Sens. Actuators B, Chem. **50**, 145 (1998).
[15] S. Patskovsky, A.-M. Dallaire, and M. Meunier, Sens. Actuators B, Chem. **222**, 71 (2016).
[16] B. M. Beam, N. R. Armstrong, and S. B. Mendes, Analyst **134**, 454 (2009).
[17] K. Imai, T. Okazaki, N. Hata, S. Taguchi, K. Sugawara, and H. Kuramitz, Anal. Chem. **87**, 2375 (2015).
[18] A. Vallee-Belisle, F. Ricci, T. Uzawa, F. Xia, and K. W. Plaxco, J. Am. Chem. Soc. **134**, 15197 (2012).
[19] J. Lu, W. Wang, S. P. Wang, X. N. Shan, J. H. Li, and N. J. Tao, Anal. Chem. **84**, 327 (2012).
[20] X. N. Shan, S. P. Wang, W. Wang, and N. J. Tao, Anal. Chem. **83**, 7394 (2011).
[21] J. M. McMahon, J. Henzie, T. W. Odom, G. C. Schatz, and S. K. Gray, Opt. Express **15**, 18119 (2007).
[22] C. H. Fan, K. W. Plaxco, and A. J. Heeger, Proc. Natl. Acad. Sci. USA **100**, 9134 (2003).
[23] F. Abelès, T. Lopez-Rios, and A. Tadjeddine, Solid State Commun. **16**, 843 (1975).
[24] B. P. Nelson, T. E. Grimsrud, M. R. Liles, R. M. Goodman, and R. M. Corn, Anal. Chem. **73**, 1 (2001).
[25] E. Reimhult, C. Larsson, B. Kasemo, and F. Hook, Anal. Chem. **76**, 7211 (2004).
[26] S. Patskovsky, V. Latendresse, A. M. Dallaire, L. Dore-Mathieu, and M. Meunier, Analyst **139**, 596 (2014).
[27] A. Barik, L. M. Otto, D. Yoo, J. Jose, T. W. Johnson, and S. H. Oh, Nano Lett. **14**, 2006 (2014).
[28] S. Patskovsky, E. Bergeron, D. Rioux, M. Simard, and M. Meunier, Analyst **139**, 5247 (2014).
[29] T. Sannomiya, O. Scholder, K. Jefimovs, C. Hafner, and A. B. Dahlin, Small **7**, 1653 (2011).